

MULTI-SCALE THERMAL-HYDRAULIC ANALYSIS OF SAFETY SYSTEMS OF ADVANCED PWRs USING THE CUPID CODE

Han Young Yoon* , Ik Kyu Park, and Chul-Hwa Song

Korea Atomic Energy Research Institute
1045 Daedeok-daero, Daejeon 305-353, South Korea
hyyoon@kaeri.re.kr; gosu@kaeri.re.kr; chsong@kaeri.re.kr

Hyoung Kyu Cho

Department of Nuclear Engineering
Seoul National University
1 Gwanak-ro, Gwanak-gu, Seoul 151-742, South Korea
chohk@snu.ac.kr

Jae Jun Jeong

School of Mechanical Engineering
Pusan National University
30 Jangjeon-dong, Geumjeong-gu, Busan 609-735, South Korea
jjjeong@pnu.ac.kr

ABSTRACT

Computer codes having different length scale are utilized to provide a high fidelity safety or performance analysis of PWRs, which is called as a multi-scale analysis. In this paper, a multi-scale thermal hydraulic analysis is introduced using CUPID and MARS which are component- and system-scale thermal hydraulics codes. The PASCAL test is simulated using the CUPID-MARS where the CUPID code has been coupled with the MARS code. PASCAL is an assessment loop of KAERI intended to validate the passive auxiliary feedwater system (PAFS) of APR+. The two-phase flow phenomena of the steam supply system including the condensation inside the heat exchanger tube were calculated by MARS while the natural circulation and the boil-off in the large water pool that contains the heat exchanger tube were simulated by CUPID. The long transient of PASCAL which lasted during 8 hours has been successfully analyzed using the coupled code. Then, a multi-scale analysis of the VAPER test is introduced. VAPER is a prototypical full-scale test facility of APR1400 advanced safety injection tank (SIT). The pressure drop inside the fluidic device is calculated in a CFD-scale. Then a component-scale pressure drop model is proposed based on the CFD-scale calculation for the simulation of the discharge transient of VAPER. Pressure, SIT water levels, and discharge flows have been accurately predicted. Analysis models are proposed for the MARS code based on the results of CUPID.

KEYWORDS

Multi-scale, coupling, CUPID, MARS

* Footnote, if necessary, in Times New Roman font and font size 10

1. INTRODUCTION

High fidelity numerical simulations are often required to address the performance of new safety systems designed for advanced pressurized water reactors (PWRs) since the safety system usually adopts passive functions where hydraulic driving force is small and multi-dimensional effects are significant. While it is not practical to compute the whole PWR system with a fine resolution in space, a multi-scale numerical simulation of a PWR [1], where computer codes having different length scales are utilized, is useful for an accurate prediction of safety system thermal hydraulic performance with reasonable computing time. For instance, in a system- and CFD-scale coupled method, the overall system behavior is simulated using a system thermal hydraulics code while the local behavior is addressed by a CFD code. The multi-scale calculation can be simultaneous or sequential. Development of a system-scale thermal hydraulics model using the simulation result of a CFD code is a one example of the sequential multi-scale calculation.

In this paper, multi-scale thermal hydraulic analyses are introduced using CUPID [2-3]. The CUPID code has been developed at KAERI for a transient, three-dimensional analysis of a two-phase flow in light water nuclear reactor components. It can provide both a component-scale and a CFD-scale simulation by using a porous media or an open media model for a two-phase flow. For a simultaneous multi-scale calculation, the CUPID code has been coupled with a system thermal hydraulic code, MARS [4]. In the coupled CUPID-MARS code, the coupling was achieved in two different ways, “flow field coupling” and “heat structure coupling”. In the flow field coupling method, the pressure matrix of both codes were unified and solved at the same time. This is called an implicit coupling method and has an advantage in transient two-phase flow simulation where the flow condition at the coupled interface changes in time [5]. On the other hand, in the heat structure coupling method, there is no fluid flow exchange at the interface; only heat transfers through. It is also called the explicit coupling method since the flow fields of both codes need not to be calculated simultaneously [6].

The multi-scale simulation using CUPID-MARS is applied to the analysis of PASCAL. The PASCAL test is an assessment loop [7] of KAERI intended to validate PAFS (passive auxiliary feedwater system) of an advanced PWR, APR+. The coupling interface between the two codes is the outer wall of the heat structure. The conduction equation for the solid interface is calculated by MARS. The two codes are coupled by sharing the heat structure surface temperatures at every time step by using the interactive control function of MARS. The two-phase flow phenomena of the steam supply system including the condensation inside the heat exchanger tube were calculated by MARS while the natural circulation and the boil-off in the large water pool that contains the heat exchanger tube were simulated by CUPID. The long transient of PASCAL which lasted during 8 hours has been successfully analyzed using the coupled code.

Then the CUPID code is applied to the analysis of the VAPER test [8] which is a prototype full-scale test facility of APR1400 advanced safety injection tank (SIT, or called accumulator) equipped with a passive flow controller, named fluidic device. In this calculation, the sequential multi-scale method has been adopted where the CUPID code was used in both CFD- and component-scale. At first, the pressure drop inside the fluidic device is calculated in a CFD-scale. Then a component-scale pressure drop model is proposed based on the CFD-scale calculation for the simulation of the discharge transient of VAPER. It has to be pointed out that, in this multi-scale analysis, different length scale codes are applied sequentially rather than using a coupled code. Calculation results are compared to VAPER data for the pressure, SIT water levels, and discharge flows. Analysis models are also proposed for the MARS code simulation of VAPER based on the results of CUPID.

2. Analysis of the PASCAL test loop using CUPID-MARS

The PAFS of APR+ is the passive auxiliary feedwater system, which is capable of condensing steam generated in a steam generator and re-feeding the condensed water to the steam generator by gravity [9]. A pool mixing test facility was constructed for the validating the cooling and operational performance of the PAFS. A single nearly-horizontal U-tube, of which dimension is same as the prototypic U-tube of the PAFS, is simulated in the pool mixing test. Fulfilment of the heat removal requirement via the PAFS has been validated and the major thermal-hydraulic parameters, such as local/overall heat transfer coefficients, fluid temperature inside the tube, wall temperature of the tube, and pool temperature distribution in the PCCT (Passive Condensate Cooling Tank), were measured [7]. In the present study, the heat structure coupled CUPID-MARS code is applied to the analysis of the pool mixing test.

The coupling interface between the two codes is the outer wall of the heat structure. The conduction equation for the solid interface is calculated by MARS. The two codes are coupled by sharing the heat structure surface temperatures at every time step by using the interactive control function of MARS. Then, designated pointer variables can be exchanged between MARS and CUPID when the latter calls the dynamic linked library (DLL) of the former. At first, the second outmost temperature of the heat structure (T_{solid}) was transferred from MARS to CUPID. With this solid temperature and the fluid temperature (T_{fluid}) at the closest fluid cell of CUPID to the wall, the wall temperature (T_{wall}) is determined from the heat transfer equation of CUPID. For sub-cooled boiling heat transfer, the following energy conservation equation [10] is solved to obtain T_{wall} :

$$\begin{aligned}
 q_{conduction} &= \frac{k_s(T_{solid} - T_{wall})}{r_{out} \cdot \ln(r_{out} / r_{in})} = q_{conv} + q_{quench} + q_{evap} & (1) \\
 q_{conv} &= h_c A_{1f} (T_{wall} - T_{fluid}), \\
 q_{quench} &= \left(\frac{2}{\sqrt{\pi}} \sqrt{t_w k_l \rho_l C_{pl} f} \right) A_{2f} (T_{wall} - T_{fluid}), \\
 q_{evap} &= N'' f \left(\frac{\pi}{6} D_{b,depart}^3 \right) \rho_g h_{fg}.
 \end{aligned}$$

This heat partitioning model is employed in order to simulate the subcooled boiling. After that, the calculated wall temperature is transferred to MARS for the boundary condition of the heat conduction equation. MARS solves the conduction equation together with the convective boundary condition imposed on the inner tube wall and the temperature distribution through the tube is obtained. Thereafter, the second outmost temperature is delivered again to CUPID for new time step calculation. This procedure is repeated in all the fluid cells of CUPID which include the heat structure for every time step.

Figure 1 shows the 1D and 2D calculation meshes of the coupled CUPID-MARS code for the simulation of the pool mixing test loop. The PCHX tube is modelled with 40 sub-nodes of MARS. The slab geometry of the PCCT is modelled in two dimensions by assuming the depth directional flow behaviours are negligible. The effect of the two planes confining the slab is considered by implementing wall friction terms in the momentum equations of CUPID. A total of 1815 (33×55) meshes are used for the present simulation.

Initially, the bottom half of the steam generator and the return-water line are filled with water and the other half, the steam supply line, and the PCHX (Passive Condensate Heat Exchanger) with steam. The initial pressure and water temperature in the primary side are 1.0 MPa and 40°C, respectively. The PCCT water level is 9.8 m and the water temperature in it is 40°C. At the right top of the PCCT, a constant atmospheric pressure boundary condition is given for the flow outlet.

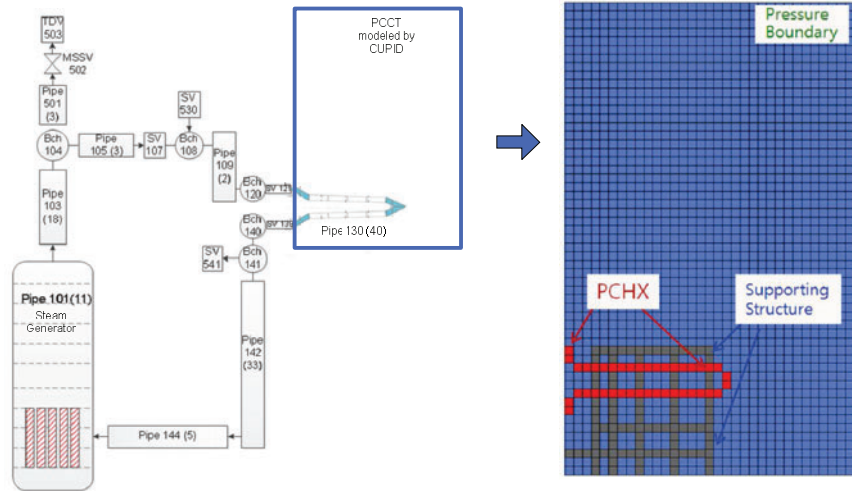


Figure 1. 1D (MARS) and 2D (CUPID) meshes for the pool mixing test loop

Figure 2 shows the calculated void fractions inside (MARS) and outside (CUPID) the PCHX, the wall vapour generation rate, and the liquid temperature distribution at 1200 seconds. The pure steam from the steam generator condenses as it flows through the PCHX and, at the outlet of the tube, the calculated void fraction is 0.86. Then the condensed water returns to the steam generator by gravity. In the PCCT, a subcooled boiling occurs on the PCHX due to the condensation heat transfer from steam as shown in Fig. 2(c). The generated vapour immediately condenses since the surrounding water is still subcooled and thus the void fraction in the PCCT is remained almost zero as indicated in Fig. 2(b). The liquid temperature outside the PCHX tube increases due to the boiling heat transfer and a single-phase natural circulation starts as shown in Fig. 2(d).

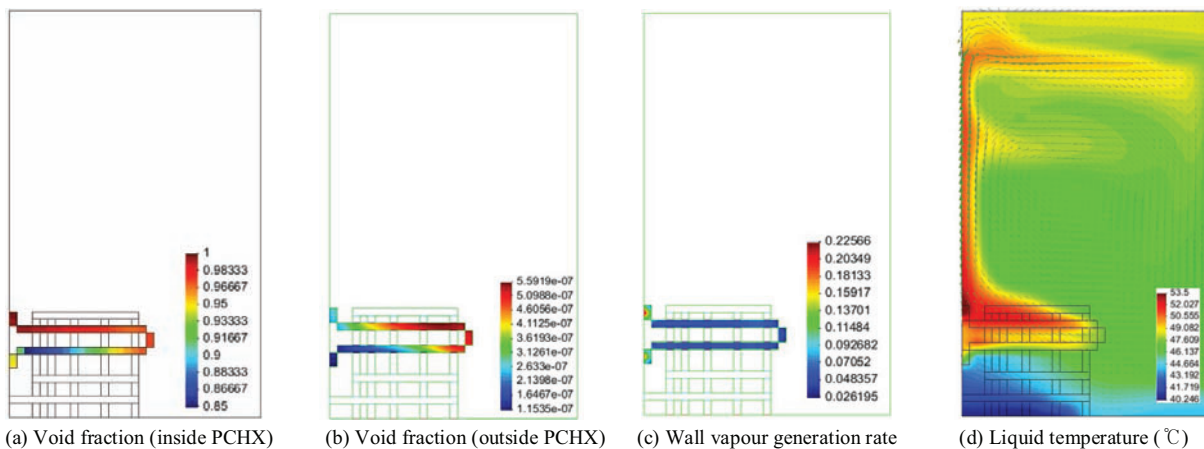


Figure 2. Calculation results at $t=1200$ sec.

The single-phase natural circulation continues until 7000 seconds from the initiation of the transient. After then, a two-phase region appears at the left side of the free surface as presented in Fig. 3. It must be noted that this phase change was induced by the flashing of the super-heated water whose temperature is 107°C but still subcooled at the elevation of PCHX due to the hydraulic head. As the heated water reaches the free surface, the pressure decreases to atmospheric pressure and vaporization occurs since now the liquid is above the saturation temperature.

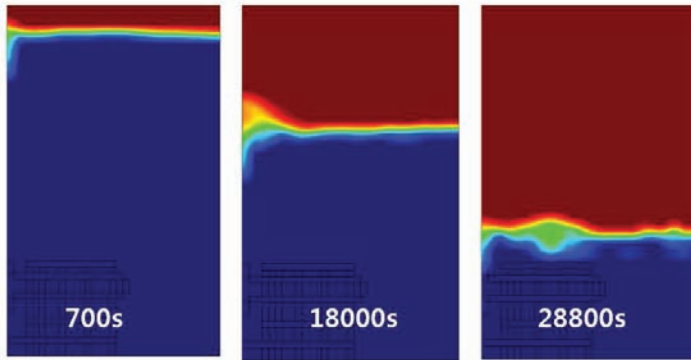


Figure 3. Water level decrease due to the boil-off

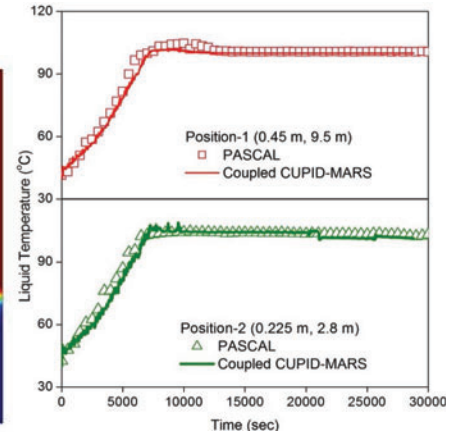


Figure 4. Liquid temperature

After the flashing, the water temperature dropped to the saturation temperature and the liquid flows downward along the other side wall and eventually, the two-phase natural circulation is established where the liquid is accelerated by bubbles, resulting in a remarkable increase of the liquid velocity. Due to the flashing near the free surface, the water level decreased gradually and reached the PCHX elevation at around 28800 seconds.

The liquid temperature transients at two different positions in the PCCT pool are compared with the experiment in Fig. 4; one is located 0.3 m below the initial free surface elevation (position-1) and the other 0.1 m below the PCHX steam inlet (position-2). The liquid temperature gradually increased from 40°C with the heat release from the PCHX and settled down as it reached the saturation temperature.

Figure 5 plotted the primary side pressure transient at the inlet of the PCHX. The system pressure increased gradually with the increasing steam generator power for the early stage of the calculation before 5,000 seconds, which is well captured by the coupled code. However, after that, the calculation under-predicts the system pressure although the decreasing trend of the pressure after 7000 seconds is well predicted. This difference is caused by the over-estimated boiling heat transfer coefficient of the heat partitioning model employed in CUPID code. The predicted boiling heat transfer rate was found to vary significantly with the bubble departure diameter model and active nucleation site density model. For example, the sensitivity analysis for the bubble departure diameter was performed and its reduction by half could increase the system pressure as comparable to the experimental result as shown in Fig. 5.

The liquid temperatures inside the PCHX at $t=13,200$ seconds are compared between the experiment and the calculation in Fig. 6. As indicated in the figure, the temperature at the bottom thermocouple (position E) is lower than the saturation temperature, while the temperature at the second one from the bottom

(position D) is slightly higher than the saturation temperature in the most of the region. This means that the condensed water level exists between two thermocouples and it is reasonable to assume that averaged liquid temperature is between the two measured temperatures. The comparison result shows that the present calculation under-predicts the liquid temperature because of the over-estimated boiling heat transfer coefficient as discussed above. The predicted liquid temperature is more close to the experiment with the modified bubble departure diameter used in the previous sensitivity analysis for primary pressure.

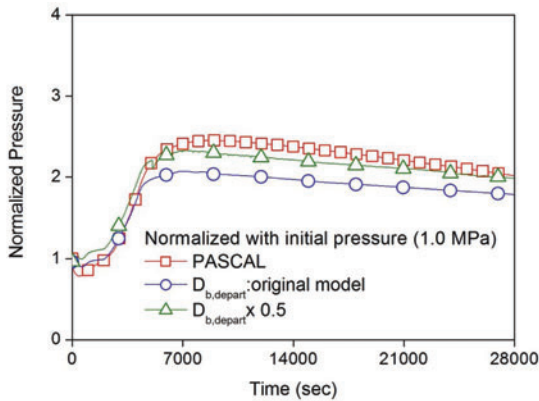


Figure 5. Primary side pressure

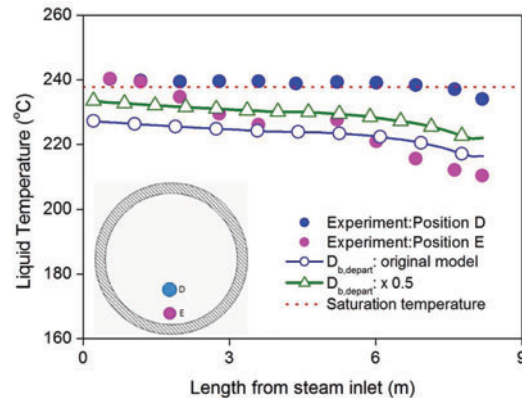


Figure 6. Liquid temperature inside PCHX tube

The long transient of the pool mixing test has been successfully simulated using the CUPID-MARS code and the important thermal-hydraulic issues related to the PAFS have been well resolved. This shows that the multi-scale thermal-hydraulic analysis using CUPID-MARS is very useful for the safety assessment of LWRs, which requires different special resolutions. Furthermore, the heat structure coupling method is easy to extend to other applications.

3. Multi-scale Analysis of the VAPER test

The advanced power reactor 1400 (APR1400), adopts a new design of safety injection system [11], consisting of four independent trains. Each train has a safety injection pump and an advanced safety injection tank (SIT, or called accumulator) equipped with a passive flow controller, named fluidic device. To evaluate the flow controlling performance of the advanced SIT, a prototypical full-scale test facility, called Valve Performance Evaluation Rig (VAPER), was constructed at KAERI. They demonstrated that the advanced SIT can passively control the discharge flow rate of emergency core cooling (ECC) water without any moving part and it satisfies the major performance requirement of the APR1400 design. In this section, a multi-scale numerical simulation of the advanced SIT of APR1400 is introduced using a component-scale code, CUPID, and a system-scale code, MARS.

3.1 Simulation using CUPID

Prediction of the water level in the standpipe is important to determine whether N_2 gas is entrained during the low flow mode, which should be avoided for a stable discharge. The water level difference between the standpipe and the SIT depends on the pressure drop of the control nozzle and initial SIT pressure. To evaluate the pressure drop through the control nozzle, a CFD-scale analysis has been carried out first as shown in Fig. 7. A two-dimensional computational domain is defined to include the control nozzle, for which 1600 quadrilateral grids are used. To simulate the low flow mode design condition, an inlet flow

boundary condition of 40.3 kg/s is assigned to the bottom face of (A), and an outlet pressure boundary condition of 0.1 MPa are set to the bottom, left, and top faces of (B). The calculated velocity profile is shown in Fig. 7(b). The pressure drop through the control nozzle is calculated to be 21.6 kPa. This result is retrieved in the next step to establish a flow resistance model in a component-scale analysis of the advanced SIT.

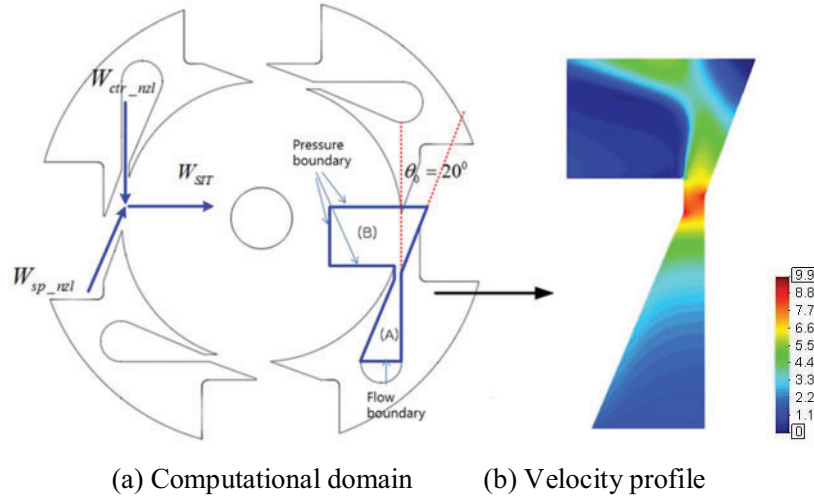


Figure 7. Pressure drop calculation

Instead of a fine scale grid, a component-scale coarse grid for the advanced SIT is developed. Because the fluid dynamics near the cylindrical wall of the advance SIT hardly affect the discharge transient, a three-dimensional rectangular column is used to model the cylindrical SIT as shown on Fig. 8(a). The number of computational grid is 17,304. The height and cross section area of the rectangular column are 11.5m and 5.90m², respectively. The cross section area is the same as that of VAPER. To simulate the pressure drop at the supply nozzle, the control nozzle, and the vortex chamber, three different regions for flow resistance are installed as shown in Fig. 8(b).

In the component-scale analysis of the advanced SIT, the pressure drops through the supply/control nozzle and the vortex chamber are calculated using a flow resistance model in the k -phase momentum equation as:

$$\frac{\partial}{\partial t}(\alpha_k \rho_k \bar{u}_k) + \nabla \cdot (\alpha_k \rho_k \bar{u}_k \bar{u}_k) = -\alpha_k \nabla P + \nabla \cdot \alpha_k \mu_k \nabla \bar{u}_k + \alpha_k \rho_k \bar{g} + \bar{F}_k^{int} + R |\bar{u}_k| \bar{u}_k \quad (2)$$

where k is liquid or gas, \bar{F}_k^{int} is interfacial momentum transfer, and R is a flow resistance coefficient.

At first, the flow resistance coefficient of the control nozzle (R_{ctr_nzl}) is determined. A flow boundary condition is assigned to the top face and a pressure boundary condition is given to the bottom face of Fig. 8(b). The flow path through the standpipe is disabled to simulate the low flow condition. The calculation is repeated to adjust R_{ctr_nzl} to get the pressure drop of the control nozzle obtained from the CFD-scale calculation mentioned in the above. The flow resistance coefficient of the vortex chamber at the low flow mode ($R_{vtx_ch_low}$) is determined so that the calculated pressure drop of the vortex chamber is equal to the design value which is given by:

$$\Delta P_{vtx_ch_low}^{design} = \frac{1}{2} K_{vtx_ch_low}^{design} \frac{W_{discharge}^2}{\rho A_{discharge_pipe}^2} \quad (3)$$

where the design form loss factor of the vortex chamber at low flow mode ($K_{vtx_ch_low}^{design}$) is 95~110. In this calculation, the nominal value of 102.5 is applied.

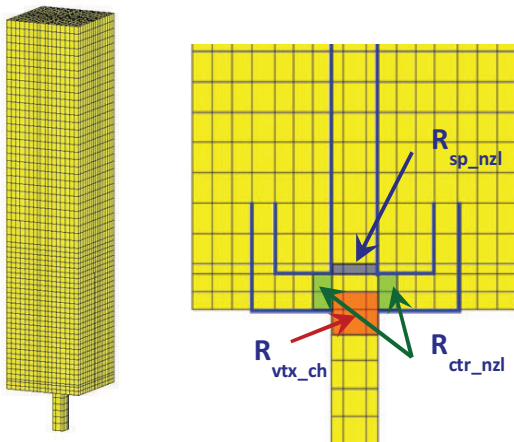
Next, the flow resistance coefficients of the supply nozzle (R_{sp_nzl}) and the vortex chamber at high flow mode ($R_{vtx_ch_high}$) are determined. The boundary conditions are given as in the same way of the low flow mode except that the flow path is available through the standpipe. R_{sp_nzl} is adjusted to obtain the following condition assuming that there is no rotational flow in the vortex chamber at the high flow mode.

$$\cos \theta_0 \cdot W_{sp_nzl} = W_{ctr_nzl} \quad (4)$$

where $\theta_0 = 20^\circ$ as shown in Fig. 7. The flow resistance coefficient of the vortex chamber at high flow mode ($R_{vtx_ch_high}$) is determined so that the calculated pressure drop of the vortex chamber is equal to the design value which is given by:

$$\Delta P_{vtx_ch_high}^{design} = \frac{1}{2} K_{vtx_ch_high}^{design} \frac{W_{discharge}^2}{\rho A_{discharge_pipe}^2} \quad (5)$$

where the design form loss factor of the vortex chamber at the low flow mode ($K_{vtx_ch_low}^{design}$) is 10~15. In this calculation, the nominal value of 12.5 is applied.



(a) Hexagonal grid (b) Flow resistance

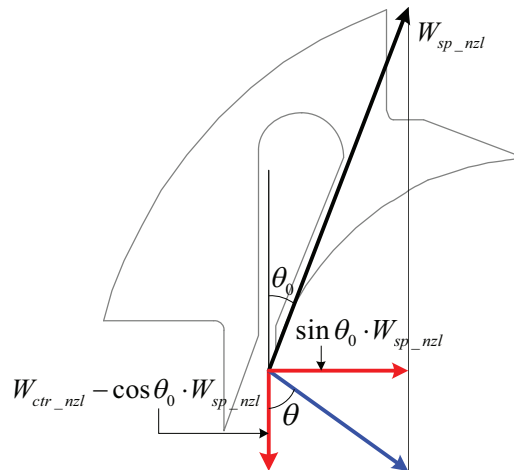


Figure 8. Computational grid and flow resistance **Figure 9. Flow momentum change**

Transient flow resistance coefficient of the vortex chamber (R_{vtx_ch}) ranging from $R_{vtx_ch_high}$ to $R_{vtx_ch_low}$ is correlated considering the fluid momentum through the supply and the control nozzles as shown in Fig. 9.

$$R_{vtx_ch} = \frac{\theta}{90} R_{vtx_ch_high} + \left(1 - \frac{\theta}{90}\right) R_{vtx_ch_low} \quad (6)$$

where θ is the angle between the control nozzle exit and the discharge flow directions which is given by:

$$\theta = \arctan \left[\frac{\sin \theta_0 \cdot W_{sp_nzl}}{W_{ctr_nzl} - \cos \theta_0 \cdot W_{sp_nzl}} \right] \quad (7)$$

At high flow mode, $\theta = 90^\circ$ since the denominator of Eq. (7) is zero by Eq. (4) and at low flow mode, $\theta = 0^\circ$ since $W_{sp_nzl} = 0$. Finally, the flow resistance coefficients obtained above are implemented into the supply nozzle, control nozzles and vortex chamber of the component-scale coarse grid, respectively.

Two cases of the VAPER experiments have been analyzed using the CUPID with the aforementioned component-scale models. Initial SIT pressures are 2.1 and 4.1 MPa, respectively. Initial water levels are the same for both cases as 89% of total height of the SIT. The calculated SIT pressure and water level of the two experiments are compared to the measured data in Figs. 10 and 11. In general, the results show excellent agreements with the measured data. This indicates that the component-scale coarse grid with the flow resistance model can represent the complicated flow structure in the passive flow control device. The water level in the standpipe was also reasonably predicted, but the undershooting was not exactly reproduced. This is not only a limitation of the approach but also the result of the trade-off between computational cost and accuracy.

Figure 12 presents the discharge flow behaviors. It is noted that, during the high flow mode in the two experiments, the discharge flow rates through the supply and control nozzles are almost the same. However, during the low flow mode, the flow rate through the supply nozzle disappears. The CUPID code predicts total discharge flow rates very well as shown in Fig. 12. The water level transient of the 2.1 MPa experiment is depicted in Fig. 13. The free surface of the SIT has been clearly captured during the transients. This indicates the inter-phase surface topology map works as intended. When the water level reaches the top of the standpipe, at around 40 seconds, small amount of gas is entrained and appears at the discharge pipe. The water level in the standpipe is soon stabilized so that the gas entrainment is not significant during the discharge transient. This is consistent with the experimental result.

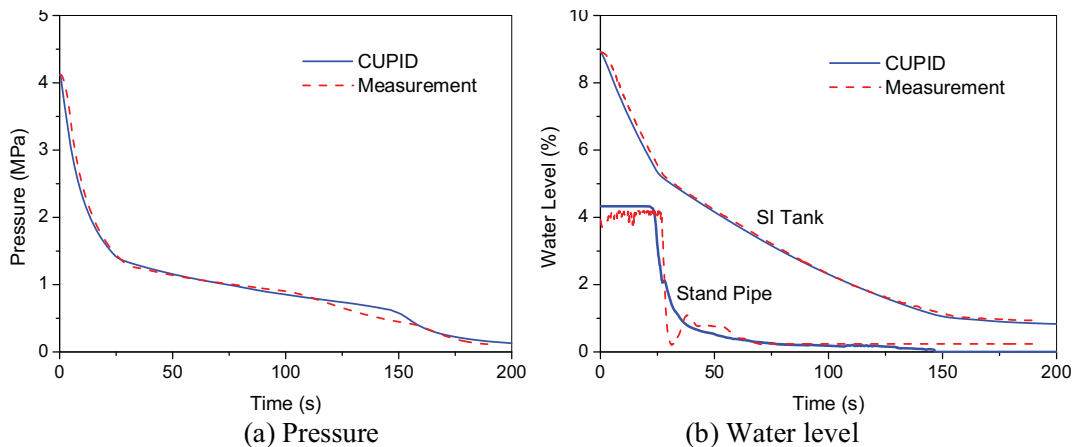


Figure 10. Comparison of the CUPID results with the experiment at 4.1 MPa

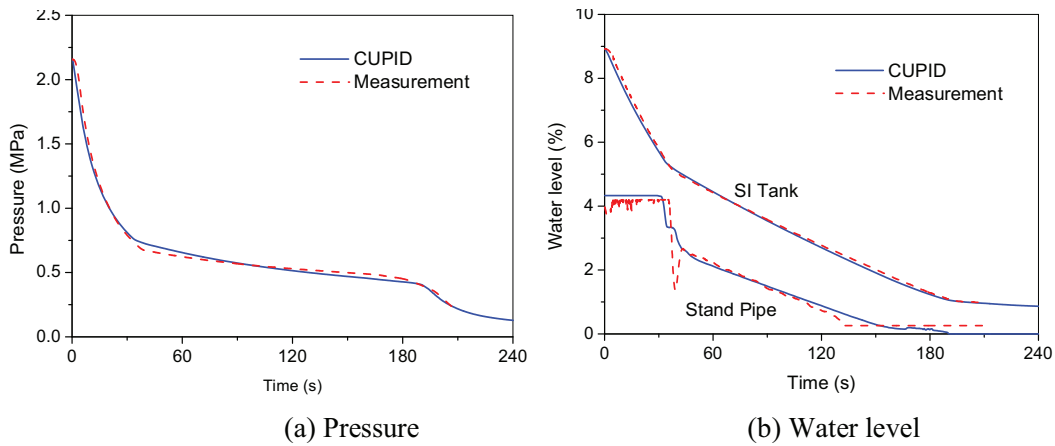


Figure 11. Comparison of the CUPID results with the experiment at 2.1 MPa.

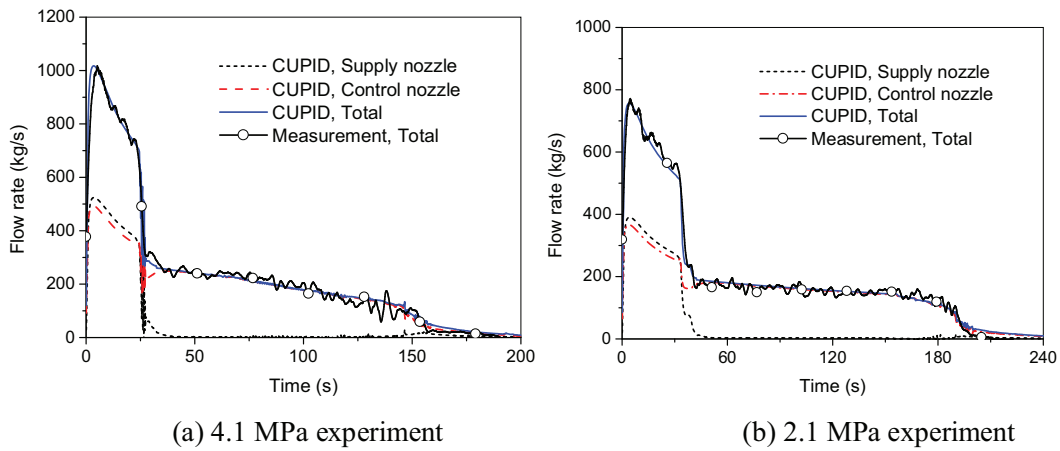


Figure 12. The discharge flow rates of the CUPID calculations.

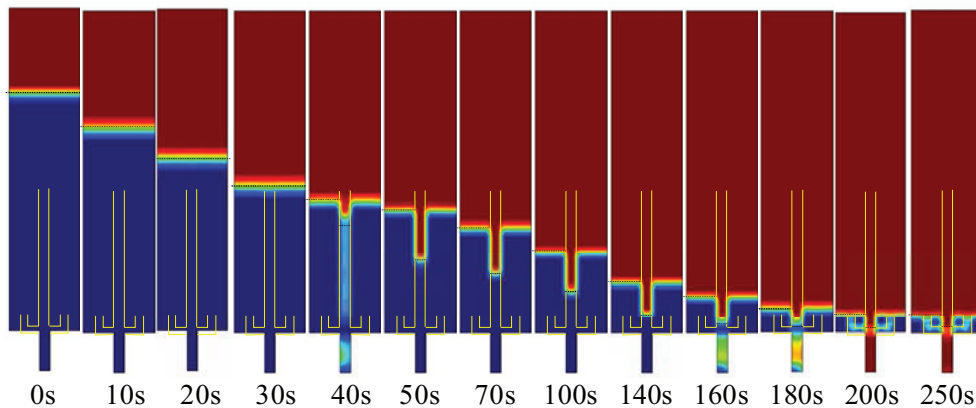


Figure 13. The water distribution in the SIT (2.1MPa); dotted lines show measured water level

3.2 Simulation using MARS

The MARS code is a best-estimate thermal-hydraulic system code, which has been developed by consolidating the RELAP5/MOD3 and COBRA-TF codes. It still maintains the general, versatile features of RELAP5/MOD3. A number of the improved features, such as a three-dimensional hydrodynamic component, have been implemented.

For the MARS simulation of the VAPER experiments, two approaches were adopted:

- Using the “accumulator” component: The lumped-parameter “accumulator” component in the MARS code is adopted, where the SIT is considered as a single volume. It adopts the assumption of an ideal gas for the upper gas volume in the SIT. Two junctions (V1 and V2) in Fig. 14(a) stand for the flow paths for the high and low flow modes, respectively. The form loss factors of V1 and V2 are obtained from the experiments; $K_{V1} = 12.5$ and $K_{V2} = 102.5$. These values were used in the CUPID flow resistance model. Only one of the two valves is open.
- Using the “pipe” component: A “pipe” component with 13 “volumes” is used to represent the SIT. Another “pipe” component is used to model the standpipe. The two-fluid model of the MARS code is applied to all the volumes without additional assumptions. Two junctions (P1 and P2) in Fig. 14(b) stand for the flow paths through the supply and control nozzles, respectively. When the water level in the SIT is lower than the top of the standpipe, the flow path through the supply nozzle (P1) is assumed to be closed. This assumption can be justified from the results of the experiments and the CUPID calculation, which are shown in Figs. 12 and 13. The SIT water level is given as a function of the water inventory. The form loss factors of the two paths are retrieved from the experimental data and the following relationship; $(1/K_{P1}^{0.5} + K_{P2}^{0.5})^2 = 1/12.5$ and $K_{P2} = 102.5$.

Because of the simplified models in the two approaches, multi-dimensional flow behavior inside the SIT cannot be simulated. Instead, global transient of pressure, water level and discharge flow from the SIT are obtained in a few seconds of the computing time.

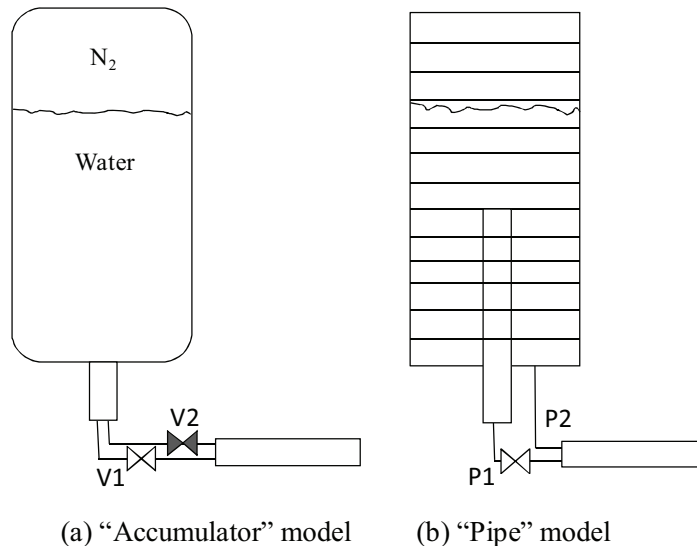


Figure 14. The MARS models for the VAPER experiment.

Two VAPER experiments conducted at the pressure of 4.1 and 2.1 MPa were simulated for this comparative study. Figure 15 shows the comparison of the MARS and CUPID results. The results of CUPID are very close to the experimental data, and the MARS “pipe” model is better next. The MARS

“accumulator” model is less accurate and physically inconsistent, yielding the slow depressurization and the rapid depletion of water inventory. This is due to the very simplified accumulator model. It is clearly shown that the overall accuracy directly depends on the computational cost and the MARS “pipe” model is cost-effective for transient analysis.

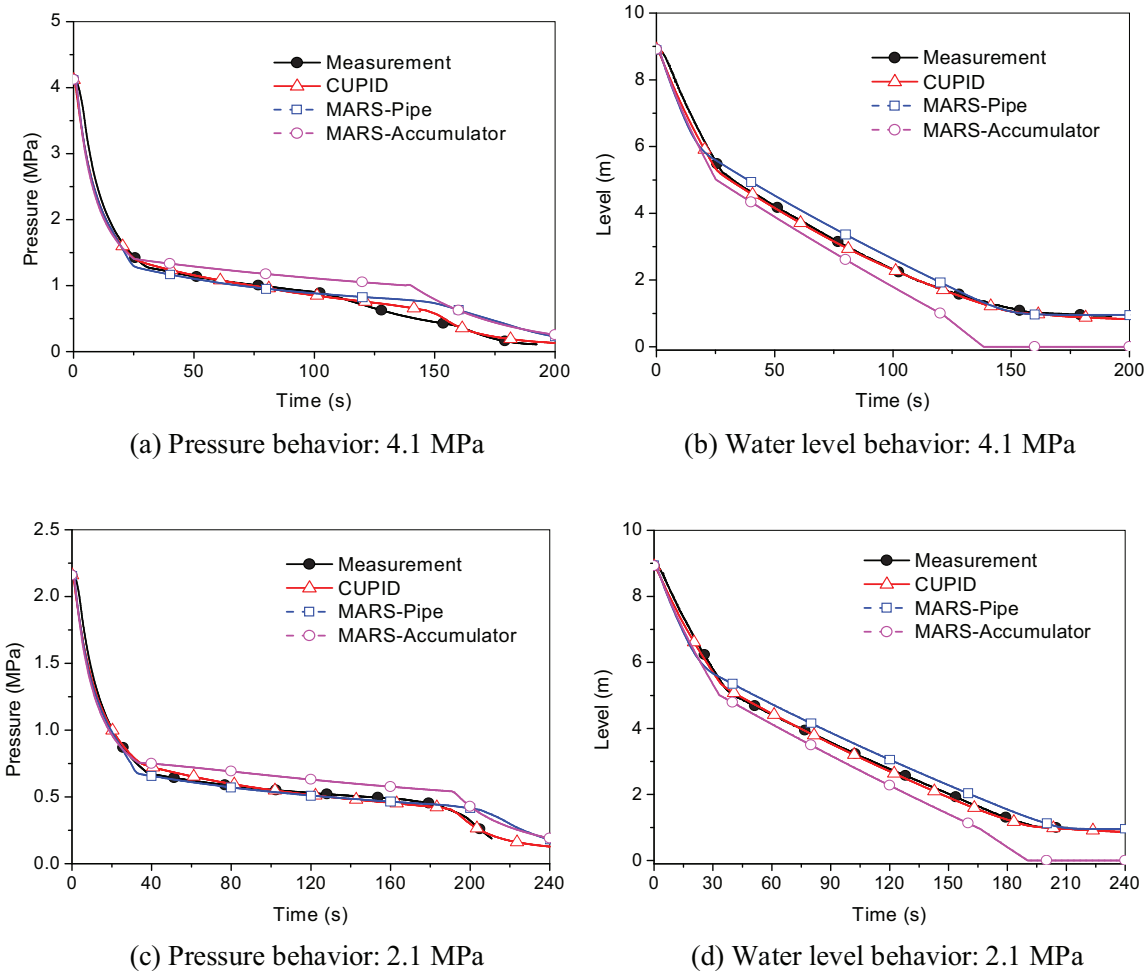


Figure 15. Comparison of the CUPID and MARS results with the experimental data.

4. CONCLUSIONS

For a multi-scale thermal hydraulics analysis of PWRs, the CUPID code has been coupled with a system analysis code, MARS. The CUPID-MARS code has been applied to the analysis of the PASCAL test. The primary side of PASCAL including the PCHX was modeled by MARS while the secondary side, the PCCS, was modeled by CUPID. The long transient of PASCAL has been successfully predicted.

The VAPER test, which is a validation experiment of APR1400 advanced SIT, has been analyzed using CUPID and MARS in CFD-, component-, and system-scale. This shows a good example of sequential application of different simulation scales compared to the coupled or simultaneous multi-scale method using CUPID-MARS. This method can be more useful since the coupled code is not needed.

The analyses showed that relevant combination of multi-scale simulations in CFD-, component-, and system-scale can provide a better solution for thermal hydraulics safety issues of PWRs. The CUPID allows different coupling methods for a practical application of the multi-scale method.

NOMENCLATURE

A_{1f} : Fraction of bubble influential area

A_{2f} : $1 - A_{1f}$

C_{pl} : Liquid heat capacity

D_b : Bubble departure diameter

f : Bubble departure frequency

\vec{F}_k^{int} : Interfacial momentum transfer rate of k -phase (k =gas, liquid)

\vec{g} : Gravity vector

h_c : Convection heat transfer coefficient

k_l : Liquid heat conductivity

k_s : Solid heat conductivity

N'' : Bubble site density

P : Pressure

R : Flow resistance coefficient

$q_{\text{conduction}}$: Conduction heat transfer rate

q_{conv} : Convection heat transfer rate

q_{quench} : Quenching heat transfer rate

q_{evap} : Evaporation heat transfer rate

r_{out} : Outer radius of PCHX tube

r_{in} : Inner radius of PCHX tube

t_w : Bubble waiting period

\vec{u}_k : Velocity vector of k -phase (k =gas, liquid)

α_k : Volume fraction of k -phase (k =gas, liquid)

ρ_k : Density of k -phase (k =gas, liquid)

μ_k : Viscosity of k -phase (k =gas, liquid)

ACKNOWLEDGMENTS

This work was supported by the National Research Foundation of Korea (NRF) and the Korea Radiation Safety Foundation (KORSAFE) grant funded by the Korean government (MSIP & NSSC) (Nuclear Research and Development Program: 2012M2A8A4025647, Nuclear Safety Research Center Program: 1305011).

REFERENCES

1. D. Bestion, "From the Direct Numerical Simulation to System Codes – Perspective for the Multi-scale Analysis of LWR Thermal hydraulics," *Nuclear Engineering and Technology*, **42**(6), pp.609-619 (2010).
2. H.Y. Yoon, H.K. Cho, J.J. Jeong, Y.S. Bang, K.W. Seul, "A Multi-scale analysis of the transient behavior of an advanced safety injection Tank," *Annals of Nuclear Energy*, vol. 62, pp. 17-25 (2013).
3. H.Y. Yoon, J.R. Lee, H.R. Kim, I.K. Park, C.-H. Song, H.K. Cho, J.J. Jeong, "Recent Improvements in the CUPID Code for a Multi-Dimensional Two-phase Flow Analysis of Nuclear Reactor Components", *Nuclear Engineering and Technology*, **46**(5), pp.655-666 (2014).
4. J. J. Jeong, K. S. Ha, B. D. Chung, and W. J. Lee, "Development of a multi-dimensional thermal-hydraulic system code, MARS 1.3.1," *Annals of Nuclear Energy*, **26**(18), pp. 1611-1642 (1999).
5. I. K. Park, J. R. Lee, S. W. Lee, H. Y. Yoon, and J. J. Jeong, "An implicit code coupling of 1-D system code and 3-D in-house CFD code for multi-scaled simulations of nuclear reactor transients," *Annals of Nuclear Energy*, **59**, pp. 80-91 (2013).
6. H. K. Cho, Y.J. Cho, H.Y. Young, "Heat Structure Coupling of CUPID and MARS for the Multi-scale Simulation of the Passive Auxiliary Feedwater System", *Nuclear Engineering and Design*, **273**, pp. 459-468, (2014).
7. K.H. Kang, B.U. Bae, S. Kim, Y.J. Cho, Y.S. Park, B.D. Kim, "Experimental Study on the Operational and the Cooling Performance of the APR+ Passive Auxiliary Feedwater System," *Proc. of ICAPP'12*, Chicago, USA, June, (2012).
8. I.C. Chu, C.-H. Song, B.H. Cho, J.K. Park, "Development of passive flow controlling safety injection tank for APR1400," *Nuclear Engineering and Design*, **238**, pp. 200-206 (2008).
9. B.U. Bae, B.J. Yun, S. Kim, K.H. Kang, "Design of condensation heat exchanger for the PAFS (Passive Auxiliary Feedwater System) of APR+ (Advanced Power Reactor Plus)," *Annals of Nuclear Energy*, **46**, pp.134-143 (2012)
10. N. Kurul, M. Z. Podowski, "On the modeling of multidimensional effects in boiling channels," *ANS Proceedings of 27th National Heat Transfer Conference*, Minneapolis, MN, USA, (1991).
11. I.S. Kim, D.S. Kim, "APR1400—development status and design features," *Proceedings of ICAPP 2002*, International Congress on Advances in Nuclear Power Plants, Hollywood, FL, June 9–13, (2002).